Crystal structure of the tyrosine kinase domain of the hepatocyte growth factor receptor c-Met and its complex with the microbial alkaloid K-252a

Nikolaus Schiering*[†‡], Stefan Knapp*, Marina Marconi*, Maria M. Flocco*[‡], Jean Cui[§], Rita Perego[¶], Luisa Rusconi[¶], and Cinzia Cristiani[¶]

Departments of *Chemistry and [¶]Biology, Pharmacia S.p.A., Discovery Research, Viale Pasteur 10, 20014 Nerviano (MI), Italy; and [§]Sugen, Inc., 230 East Grand Avenue, South San Francisco, CA 94080

Communicated by Gregory A. Petsko, Brandeis University, Waltham, MA, July 2, 2003 (received for review February 20, 2003)

The protooncogene c-met codes for the hepatocyte growth factor receptor tyrosine kinase. Binding of its ligand, hepatocyte growth factor/scatter factor, stimulates receptor autophosphorylation, which leads to pleiotropic downstream signaling events in epithelial cells, including cell growth, motility, and invasion. These events are mediated by interaction of cytoplasmic effectors, generally through Src homology 2 (SH2) domains, with two phosphotyrosine-containing sequence motifs in the unique C-terminal tail of c-Met (supersite). There is a strong link between aberrant c-Met activity and oncogenesis, which makes this kinase an important cancer drug target. The furanosylated indolocarbazole K-252a belongs to a family of microbial alkaloids that also includes staurosporine. It was recently shown to be a potent inhibitor of c-Met. Here we report the crystal structures of an unphosphorylated c-Met kinase domain harboring a human cancer mutation and its complex with K-252a at 1.8-Å resolution. The structure follows the well established architecture of protein kinases. It adopts a unique, inhibitory conformation of the activation loop, a catalytically noncompetent orientation of helix αC, and reveals the complete C-terminal docking site. The first SH2-binding motif ([1349]YVHV) adopts an extended conformation, whereas the second motif ([1356]YVNV), a binding site for Grb2-SH2, folds as a type II β-turn. The intermediate portion of the supersite ([1353]NATY) assumes a type I β-turn conformation as in an Shc–phosphotyrosine binding domain peptide complex. K-252a is bound in the adenosine pocket with an analogous binding mode to those observed in previously reported structures of protein kinases in complex with staurosporine.

Hepatocyte growth factor/scatter factor (HGF/SF)-c-Met signaling is the center of interest for many laboratories due to its importance for both embryonic development, and, when dysregulated, tumorigenesis, particularly in the development of invasive and metastatic phenotypes (1). The original identification of an N-terminal-truncated oncogenic met version on treatment of a human osteosarcoma cell line with the carcinogen *N*-methyl-*N*′-nitro-*N*-nitrosoguanidine led Cooper *et al*. to suggest the abbreviation "met" for this transforming gene (2). c-Met was subsequently shown to be a receptor tyrosine kinase (RTK) and the receptor for HGF/SF (3–5). It is the most thoroughly studied member of a small subfamily of RTKs that also includes Ron and Sea. With no orthologs identified in *Drosophila melanogaster* or *Caenorhabditis elegans*, c-Met is thought to be unique to vertebrates (6).

c-Met is an α–β heterodimer with an extracellular α-chain disulfide linked to the membrane-spanning β-chain (1,390 residues) harboring the intracellular tyrosine kinase domain. Kinase activation is achieved through autophosphorylation of tyrosines 1234 and 1235 in the activation loop (A loop) (7, 8). Perhaps the most striking characteristic of this RTK subfamily is the presence of a conserved tandem-tyrosine containing multifunctional docking site at the C terminus (supersite; in c-Met: [1349]YVHVNAT[1356]YVNV) established to be absolutely required for c-Met signaling both *in vitro* and *in vivo* (9, 10). Knock-in mice with phenylalanine substitutions of these tyrosines lead to an embryonically lethal phenotype that resembles that of c-met or HGF knockout animals, presenting placental, liver, muscle, and nerve defects (11). On activation, Tyr-1349 and Tyr-1356 become autophosphorylated and serve as docking sites for a wide spectrum of transducers and adaptors, including PI3K, Src, Grb2, Shc, Gab1, and Stat3 (12). Binding is accomplished in general through interaction with Src homology 2 (SH2) domains, and, in some instances, through Met-binding (Gab1) and phosphotyrosine-binding (PTB) (Shc; ref. 13) domains of the binding partners. The resulting multiprotein signaling complex triggers the intracellular downstream effects, including cell proliferation, scattering, and inhibition of apoptosis. c-Met gene amplification and/or protein overexpression are frequently found in a number of human carcinomas. In addition, germ-line and somatic missense mutations in the c-Met kinase domain have been identified in papillary renal and hepatocellular carcinoma, as well as in lymph node metastases of head and neck squamous cell carcinoma (HNSC) (for reviews, see refs. 1, 6, and 14). These mutations, which render the kinase constitutively active, provide compelling evidence for the link between HGF receptor signaling and cancer and make c-Met a bona fide drug target.

Staurosporine is a potent, nonselective protein kinase inhibitor, the first of >50 alkaloids with an indolocarbazole subunit isolated to date (15). Structures of staurosporine in complex with the Ser/Thr kinase domains of CDK2 and protein kinase A (PKA), as well as the tyrosine kinase domains of CSK and Lck, have been reported (16–19). They revealed a common binding mode in the adenosine cleft, induced conformational changes of the enzyme to accommodate the large compound through a complementary apolar interaction surface, and specific hydrogen-bonding interactions (for recent reviews on kinase structure and inhibition, see refs. 20 and 21).

The staurosporine analog K-252a is a potent inhibitor of a number of Ser/Thr kinases and the Trk-family of RTKs (22, 23). It was recently shown to potently inhibit also c-Met autophosphorylation, HGF-mediated cell scattering, as well as c-Met-driven proliferation in gastric carcinoma cells, and reported to cause reversion of tumorigenicity in fibroblasts transformed with an oncogenic form of c-Met (24). Here we report the crystal structures of a kinase domain of apo-Met and its complex with K-252a at 1.8-Å resolution.

Methods

Expression, Purification, and Characterization. c-Met residues 1049–1360 were cloned into the vector PVL1393 (Pharmingen), mod-

Abbreviations: HGF, hepatocyte growth factor; SH2, Src homology 2; PTB, phosphotyrosine binding; PKA, protein kinase A; FGFRK, fibroblast growth factor receptor kinase; A loop, activation loop; IRK, insulin receptor kinase; IRK3P, triple-phosphorylated IRK; ITC, isothermal titration calorimetry; MBD, met-binding domain.

Data deposition: The atomic coordinates and structure factors have been deposited in the Protein Data Bank, www.rcsb.org (PDB ID codes 1R0P and 1R1W).

[†]Present address: Novartis Pharma AG, WKL-127.P.72, CH-4002, Basel, Switzerland.

[‡]To whom correspondence should be addressed. E-mail: nikolaus.schiering@pharma.novartis.com or maria.flocco@pharmacia.com.

ified by insertion of GST, a PreScission cleavage site and a Kozak sequence. Of the three major phosphorylation sites, Tyr-1194 and Tyr-1234 were mutated into phenylalanine, and Tyr-1235 was mutated to aspartate to obtain an active form of the kinase (25) by using the QuikChange site-directed mutagenesis kit (Stratagene). An additional conservative mutation (V1272L) was present in the cDNA template used. Recombinant c-Met was expressed by using High-five insect cells (Invitrogen) and purified by GSH affinity chromatography in 50 mM Tris, pH 7.4/50 mM NaCl/10% glycerol/20 mM DTT. The GST tag was removed by using PreScission protease (Amersham Biosciences) and the recombinant protein was passed over a Resource Q column equilibrated in 50 mM Tris, pH 8.5/50 mM NaCl/3 mM DTT. The flow-through contained the purified protein, which was >95% pure as judged by SDS/PAGE and was found homogeneous and unphosphorylated by mass spectrometry. The specific activity of the mutated protein was comparable with wild-type c-Met by using gastrin as substrate. Details of the construct design and characterization will be published elsewhere.

Crystallization. Crystals of apo-Met and the complex with K-252a were obtained by using the hanging drop method and a protein concentration of 10 mg/ml. After optimization, crystals of apo-Met were prepared by mixing 1 μl of the protein in 50 mM Tris, pH 8.5/150 mM NaCl/10% glycerol/3 mM DTT with the same volume of reservoir solution [6–10% polyethylene glycol (PEG) 5000 monomethyl ether/100 mM Hepes, pH 7.1/11% isopropanol]. Employing streak seeding at day 1, crystals grew within a few days to $\approx 0.2 \times 0.06 \times 0.02$ mm^3 at 4°C. K-252a was purchased from Calbiochem. The complex was cocrystallized, adding the DMSO-solubilized compound at a 1.5-fold molar excess.

Data Collection and Structure Solution. Diffraction images were collected at the European Synchrotron Radiation Facility (Grenoble, France) beamline ID14-2. The crystals were stabilized in mother liquor containing 15% glycerol before freezing in liquid nitrogen. Raw data were reduced with DENZO (26) and scaled and merged by using SCALEPACK (ref. 26 and Table 1). The structure of the K-252a complex was solved by molecular replacement by using the program EPMR (27) and atomic coordinates of another inhibitor complex of c-Met as a starting model (unpublished data). Interactive model building with the program O (28) was alternated with refinement by using CNX (29) employing simulated annealing, the maximum likelihood target, bulk solvent correction, and restrained B factor refinement. Final rounds of refinement were performed with REFMAC (30), and water molecules were added by ARP (31). Throughout, 5% of the reflections were kept separate for crossvalidation. Refinement of apo-Met was initiated by using as a starting model the refined coordinates of the K-252a complex and was pursued by using an analogous protocol. In apo-Met, 93.5% of the residues are in the most favored region of the Ramachandran plot (K-252a: 92.4%; ref. 32). Statistics for the final models are included in Table 1.

Isothermal Titration Calorimetry (ITC) Affinity Measurements. ITC measurements were carried out as reverse titrations by using a MicroCal VP-ITC calorimeter. A 100-μM solution of c-Met mutant FFD in PBS and 1 mM DTT was titrated into a 10-μM solution of K-252a prepared in the same buffer. Dilution heats were determined by blank titrations and were subtracted from the normalized dilution heat data. Data were fitted to a single-site model by using the ORIGIN software package and fitting routines provided with the instrument.

Table 1. Data collection and refinement statistics

Data collection statistics		
Data set	Apo	K-252a
Space group	$P2_12_12_1$	$P2_12_12_1$
Unit cell dimensions, Å		
a	43.038	42.969
b	46.029	46.247
c	158.448	158.379
Resolution range, Å	30–1.8	30–1.8
Total reflections (unique)	168,428 (28,705)	144,096 (29,021)
Completeness (final shell), %	95.7 (90.4)	96.0 (89.2)
R_{merge}* (final shell)	0.084 (0.315)	0.043 (0.079)
Refinement statistics		
Resolution range, Å	30–1.8	30–1.8
Reflections (test set)	27,250 (1,405)	27,533 (1,436)
R factor† (R_{free}), %	17.29 (20.38)	16.95 (19.73)
No. of protein atoms	2,282	2,393
No. of ligand atoms	—	35
No. of water molecules	235	203
rms deviation from ideal		
Bond length, Å	0.011	0.012
Bond angle,°	1.290	1.810
Average B factors, Å^2		
Overall	19.19	12.92
Main chain	17.52	11.51
Side chain	19.56	13.56
Ligand	—	9.65
Solvent	25.66	18.16

*$R_{merge} = \Sigma_{hkl}\Sigma_i | I_{hkl} - \langle I_{hkl}\rangle | / \Sigma_{hkl}\Sigma_i(I_{hkl})$
†*R* factor $= \Sigma_{hkl}||F_{obs}| - |F_{calc}|| / \Sigma_{hkl}|F_{obs}|$

Results and Discussion

The c-Met kinase domain follows the bilobal protein kinase architecture with an N-terminal, mainly β-sheet-containing domain linked through a hinge segment to the mainly α-helical C lobe (Fig. 1*a*). The sequence identities with the kinase domains of insulin receptor kinase (IRK) and fibroblast growth factor receptor kinase (FGFRK) are >40% (IRK: 44%; FGFRK: 41%) and c-Met superimposes with a high degree of overlap with these kinases. Superpositions of the c-Met:K-252a complex yield the following rms deviations: FGFRK: 1.2 Å with Protein Data Bank (PDB) ID code 1FGI, chain A (222 C^α pairs; ref. 33) and 1.3 Å with PDB ID code 1FGK, chain B (232 C^α pairs; ref. 34); IRK: 1.5Å with PDB ID code 1IRK (216 C^α pairs; ref. 35) and 1.6Å with PDB ID code 1IR3 (226 C^α pairs; ref. 36), as well as with apo-Met: 0.5 Å for 296 C^α positions.

The closest structural similarity is with FGFRK (34), where, in addition to almost the entire C lobe, the majority of the N-lobe secondary structure elements also superimpose closely. The largest difference between these structures in the N lobe is found for helix αC (nomenclature according to ref. 37). In c-Met, the N-terminal portion of αC is pushed away from the C lobe with these helices forming an angle of $\approx$20° in the superimposed structures from the pivot point at the residue pair 1134 (c-Met)-538 (FGFRK). The difference in the orientation of $^\alpha$C is even more pronounced when comparing c-Met with the active conformation of the insulin receptor [triple-phosphorylated IRK (IRK3P)] (36), where an angle of $\approx$30° from the residue pair 1134 (c-Met)-1054 (IRK3P) toward the N terminus of the helix is observed. αC in the inactive conformation of insulin receptor [nonphosphorylated IRK (IRK0P)] (35), on the other hand, assumes a similar relative orientation with respect to the kinase body as observed in c-Met. The salt bridge between residues Lys-1110 (β3) and Glu-1127 ($^\alpha$C) expected to be present in the active kinase conformation is not observed in the two c-Met structures described here (Fig. 1*b*).

BIOCHEMISTRY

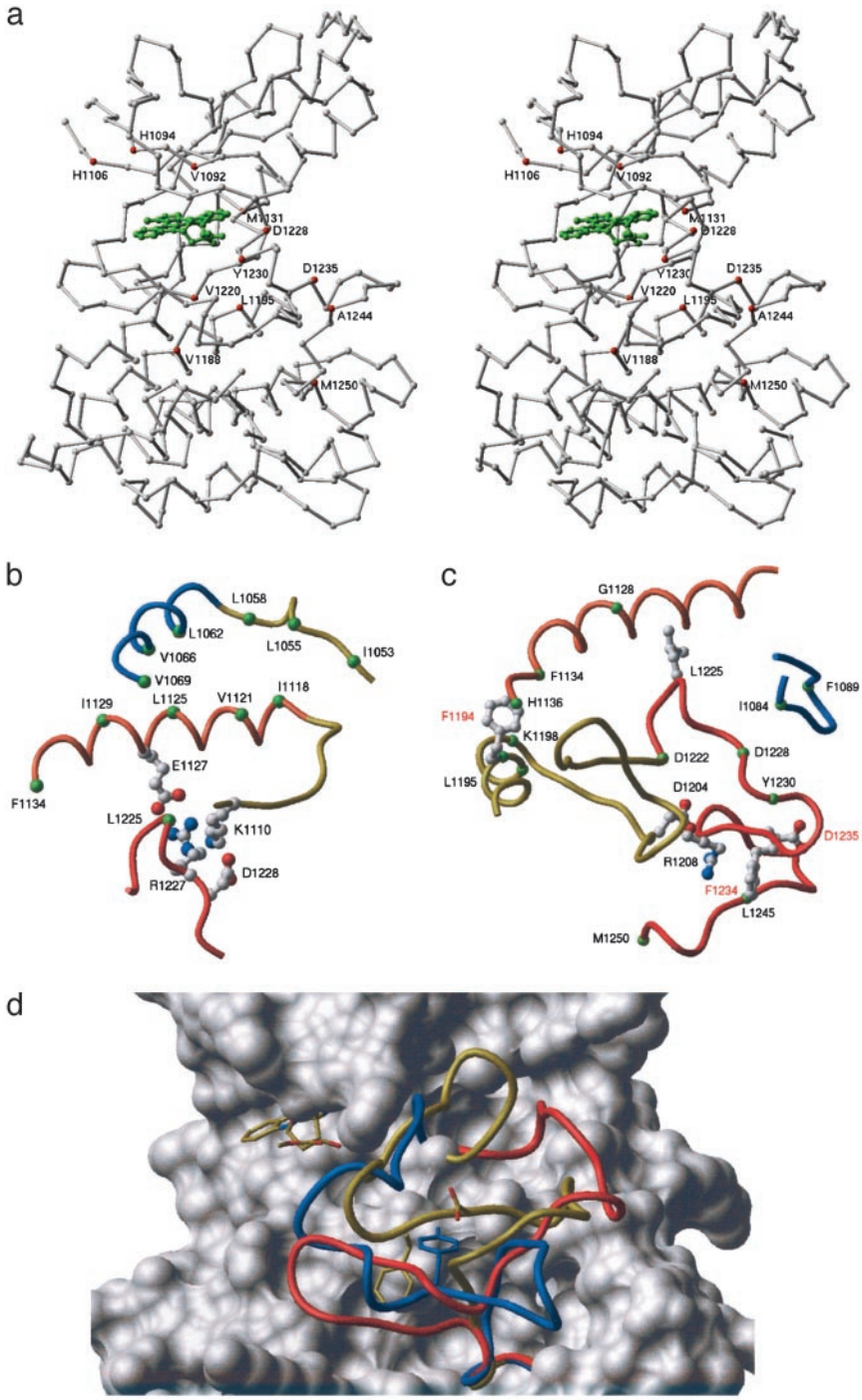

Fig. 1. (*a*) C^{α} plot of c-Met in complex with K-252a. The inhibitor is green. The model extends from residues 1050 to 1360. Disordered and not included in the model are residues 1100–1103 (apo-Met: 1099–1103) and residues 1286–1291 (1286–1290), as well as the A-loop residues 1231–1244 in apo c-Met. Residues mutated in human cancer are highlighted with their C^{α} atoms in red. (*b*) A view of parts of the N lobe and the A loop. Carbonyl carbon positions of residues mentioned in the discussion are shown as green spheres. αA is blue, αC is orange, their flanking regions (including part of β3 that precedes αC) are yellow, and the N-terminal portion of the A loop is red. (*c*) A view of the domain interface as in *b*. The glycine-rich loop is blue, αC is orange, residues 1190–1221 (including the C terminus of αE and the catalytic loop) are yellow, and the A loop is red. Red labels indicate the residues mutated in our study. (*d*) Surface of c-Met:K-252a with the A loop shown as a yellow ribbon. Also shown are parts of the bound inhibitor, as well as side chains for Phe-1234 and Asp-1235. For comparison, the A loops in IRK0P (blue; also shown is Y1162, PDB ID code 1IRK; ref. 23) and FGFRK (red; PDB ID code 1FGI; ref. 43) are shown. All figures were prepared by using ICM (44).

At the N terminus of the structure, before the core kinase domain, residues 1060–1069 form a helix (1067–1069: 3_{10} helix) not present in FGFRK or IRK. The C terminus of αA in PKA is close to the C terminus of this helix in c-Met, but these helices extend toward the N terminus in opposite directions. In c-Met, αA packs at a slight angle and with parallel directionality against αC, with residues Leu-1062, Val-1066, and Val-1069 intercalating with Leu-1125 and Ile-1129 from αC (Fig. 1*b*). The interface is augmented by interactions between the side chains from Ile-1118 and Val-1121 from αC that pack against Ile-1053, Leu-1055, and Leu-1058 from the N-terminal c-Met segment preceding αA. A reorientation of αC during the transition to an active kinase conformation will hence need to be in concert with a movement of this segment N-terminal to the core kinase domain and ≈100 residues downstream from the membrane-spanning portion of the c-Met β-chain. Helix αA could therefore be part of the structural elements involved in the kinase activation on ligand binding to the extracellular portion of c-Met. An orientation of αC, as found in FGFRK or IRK3P, would lead to steric clashes with the N terminus of the A loop.

The c-Met A loop adopts a unique conformation beyond residue Phe-1223 of the DFG motif. Residues 1223–1226 bulge up toward the N lobe, adopting a type II′ β-turn conformation with residues Gly-1224 and Leu-1225 at the center of the turn.

At the apex of this bulge toward the N-lobe is Leu-1225, of which the side chain is in van der Waals distance to Gly-1128 approximately at the center of αC (Fig. 1*c*). Apo-Met and the K-252a complex adopt the same conformation for the A-loop residues Asp-1222–Arg-1227. Due to induced conformational changes on inhibitor binding, there is, however, a significant divergence for the A-loop portion including residues Asp-1228, Met-1229, and Tyr-1230 (see below). In both structures, the segment 1229–1230 passes through the triphosphate subsite of bound ATP, as derived by analogy, from its position in IRK3P. Hence, residues 1222–1230 assume an inhibitory conformation both with respect to constraining αC into an orientation that does not allow proper catalytic positioning of Glu-1127 and by inhibiting nucleotide binding.

In the apo-Met structure, A-loop residues 1231–1244 are not defined by electron density, whereas in the K-252a complex, the entire A loop is ordered. In wild-type c-Met, tyrosines 1234 and 1235 become phosphorylated on receptor activation (7). In our crystallographic studies, we used a mutant where these tyrosines were substituted with phenylalanine and aspartate, respectively. Y1235D is a mutation described in metastatic HNSC carcinoma, leading to an increase in c-Met kinase activity and conferring an invasive phenotype to transformed cells (25). The third mutated residue is Tyr-1194, which was exchanged for phenylalanine. Phe-1194 points into a pocket formed by residues Lys-1198 and Leu-1195, both also originating from αE, as well as His-1136 and Phe-1134 at the C terminus of αC (Fig. 1*c*). As in wild-type c-Met, in IRK and FGFRK there is a tyrosine in the position structurally corresponding to residue 1194. This region is structurally conserved, indicating that this mutation does not disturb the local structure of c-Met. It is conceivable that a phosphorylation of Tyr-1194 contributes to the formation of an active c-Met kinase structure by contacting the pivot point of the αC hinge motion. By introducing these three mutations, we obtained homogenous nonphosphorylated protein retaining enzymatic activity.

A-loop residues 1231–1244 in the K-252a complex adopt a conformation different from that of other active or inactive kinases (IRK0P, IRK3P, and FGFRK, and Fig. 1 *c* and *d*). This segment is in an inhibitory conformation, with the protein chain occluding the area of substrate peptide binding. The main chain of residues Phe-1234 and Asp-1235 passes approximately through the position where the substrate tyrosine side chain would be expected to bind in an active conformation of the kinase (Tyr-B10 in IRK3P). The A-loop segment 1230–1244 forms three strand-like sections, with Asp-1235 located on the middle one, which is close to the center of this portion of the structure. Its side chain interacts with the amide nitrogens of Ala-1243 and Ala-1244. The side chain of Phe-1234 is in a stacking interaction with two conserved residues, Arg-1208 and Trp-1249 (Fig. 1*c*). Mroczkowski *et al.* (45) disclosed the structure of wild-type, unphosphorylated c-Met in complex with an oxindole inhibitor bound in the ATP cleft in a patent application. In that structure, residues 1223–1227 adopt a bulged conformation as in our c-Met structures, indicating that this conformation is a unique structural feature of c-Met, which is not influenced by the mutations Y1234F and Y1235D we introduced in the A loop. The conformation observed in the K-252a complex could nevertheless be a relevant state during the transition to an active A-loop structure.

Binding of K-252a. K-252a differs from staurosporine in the glycosyl portion, having a furanose, rather than a pyranose moiety (Fig. 2*a*). The furanose of K-252a is substituted in 3′ with a hydroxyl group and a methoxycarbonyl group, and in 4′ with a methyl function. We determined, by ITC, a dissociation constant of 10 nM for this compound. In addition, the ITC data revealed an unusually large favorable binding enthalpy change of

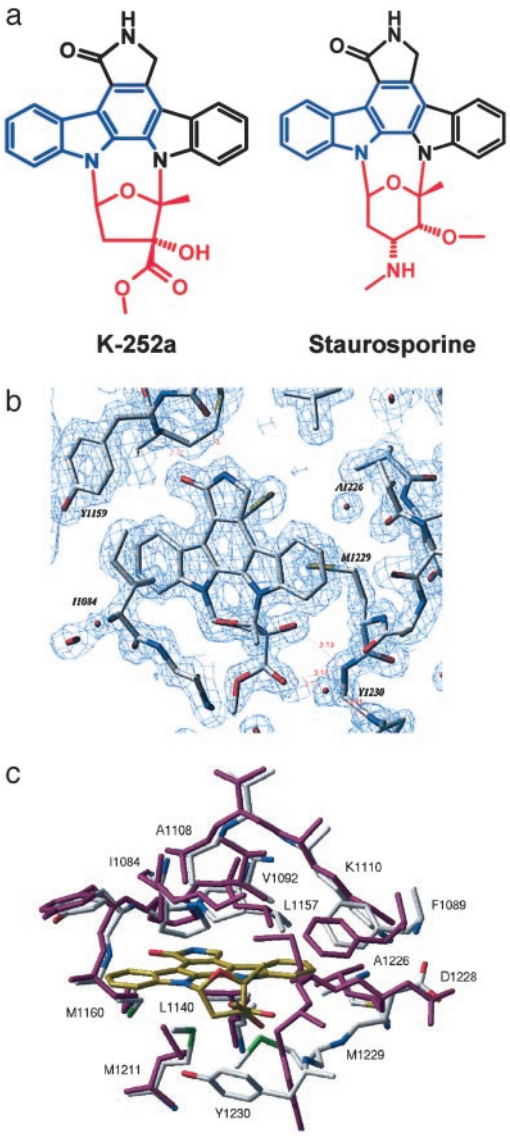

Fig. 2. (*a*) Chemical structures of K-252a and staurosporine. The carbazole ring system is blue, and the sugar moieties (pyranose in staurosporine and furanose in K-252a, respectively) are red. The lactam and indole rings are black. (*b*) $2F_o$-F_c electron density map of the K-252a-binding site contoured at 1.5σ. Hydrogen bonds are indicated. (*c*) c-Met inhibitor binding site. Carbon atoms of c-Met:K-252a are gray and apo-Met atoms are magenta. Carbonyl oxygens were omitted for clarity. K-252a carbons are yellow.

−17.9 kcal/mol, implying favorable polar interactions, as well as conformational changes on inhibitor binding.

K-252a binds in the adenosine pocket of c-Met with an analogous binding mode to that reported for staurosporine in several kinase complexes (refs. 16–19 and Fig. 2*b*). The indolocarbazole moiety, lactam ring, and glycosyl-oxygen of CDK2-, PKA-, Csk- and Lck-bound staurosporine are in close proximity to the corresponding moieties of K-252a when the kinase structures are superimposed on the hinge region. K-252a makes four hydrogen bonds to enzyme residues and one hydrogen bond to a water molecule. Two hydrogen bonds, as in the staurosporine complexes, anchor the lactam moiety to the hinge region and mimic the hydrogen bonding pattern of the adenine base in protein kinase:adenosine nucleotide complexes. The lactam amide nitrogen donates a hydrogen bond to the carbonyl oxygen of residue Pro-1158. The lactam carbonyl oxygen accepts a

hydrogen bond from the main-chain amide of Met-1160. In apo-Met, one water molecule is present at the position of the lactam nitrogen and another water molecule is close to the position of the lactam oxygen. Water molecules in the corresponding positions have also been reported for apo-CDK2 (17). Three additional hydrogen bonds, unique to this complex, are formed with atoms from the K-252a furanose moiety. The carbonyl oxygen and the 3′ hydroxyl make hydrogen bonds to the main-chain nitrogen of Tyr-1230 in the A loop. A bridging water molecule links the K-252a carbonyl oxygen with the carbonyl oxygen of Asp-1228, the main-chain nitrogen of Tyr-1230, and the carboxylate oxygen of Asp-1231. In apo-Met, this water molecule is not present because of a different conformation of the main chain at this position (see below).

A large number of hydrophobic contacts between K-252a and the enzyme are present in the complex, with a high complementarity between the interacting surfaces (Fig. 2*c*). Residues lining the binding pocket that are involved in this apolar interface are Ile-1084, Gly-1085, Phe-1089, Val-1092, Ala-1108, Lys-1110, and Leu-1140 (from the N lobe); Leu-1157, Pro-1158, Tyr-1159, and Met-1160 (from the hinge region); and Met-1211, Ala-1226, Asp-1228, Met-1229, and Tyr-1230 (from the C lobe). Phe-1089 assumes an inwardly bent rotamer conformation contacting the sugar-methyl group in the same way as found for Phe-54 in the PKA:staurosporine complex.

The side chains of Met-1211, together with those of Met-1160 and Met-1229 that flank it in van der Waals distance, build a platform for the bottom of the indolocarbazole plane. Major K-252a-induced conformational differences between the apo and complex structures concern the N-terminal portion of the A loop, residues Asp-1228, Met-1229, and Tyr-1230. The side chain of Met-1229, as oriented in apo-Met, would pass through the hinge-distal six-membered ring of the indolocarbazole moiety. To make room for the alkaloid, the main chain moves by 3.8 and 3.1 Å for the C^{α} positions of Met-1229 and Tyr-1230, with the side chains moving by 5.5 (SD Met-1229) and 6.8 Å (OH Tyr-1230). Arg-1208, which in apo-Met stacks with the phenolic side chain of Tyr-1230, moves its side chain in the complex by 8 Å (CZ atoms) toward the catalytic base, Asp-1204, to free the space for the side-chain position of Tyr-1230 in the K-252a complex. In its new position, which corresponds to the one observed for this conserved arginine residue in IRK and FGFRK, Arg-1208 stacks with its guanidinium portion against the benzyl ring of Phe-1234 (wild-type Tyr-1234) in the A loop (Fig. 1*c*). This concerted reorientation in the K-252a complex might contribute to the ordering of the C-terminal portion of the A loop. Residues 1084–1089 from the glycine rich loop close down toward the upper surface of the indolyl carbazole ring system, undergoing a main-chain displacement of up to 2.7 Å. The α-carbon of Gly-1085 approaches the K-252a glycosyl oxygen by 1.2 Å to a distance of 3.7 Å, making a CH-O interaction possible. The same interaction was identified by Zhu *et al.* (19) for protein kinase:staurosporine complexes. Unlike PKA and CDK2, where staurosporine binding is accompanied by an opening of the relative orientation of the N and C lobes, we observe a lobe closure of ≈3° in the K-252a complex, compared with the apoform of the kinase.

C-Terminal Docking Site. In c-Met, the C-terminal tail sequence ^{1349}YVHVNAT^{1356}YVNV contains the two tyrosines, which, after phosphorylation, act as docking sites for a multitude of intracellular signal transducers through interactions with SH2, MBD, and PTB domains. Whereas the majority of the SH2-containing binding partners are reported to bind to both motifs, ^{1356}YVNV is a consensus-binding site for the Grb2 SH2 domain. In general, phosphotyrosine-containing peptides bind to SH2 domains in an extended conformation (38). Grb2 SH2 is the only SH2 domain reported to date that binds the peptides in a type I β-turn conformation with the asparagine residue in the position pY + 2 forming two hydrogen bonds with the SH2 domain (39, 40). The bulky Trp-121 side chain in the EF loop of Grb2-SH2 excludes an extended peptide conformation.

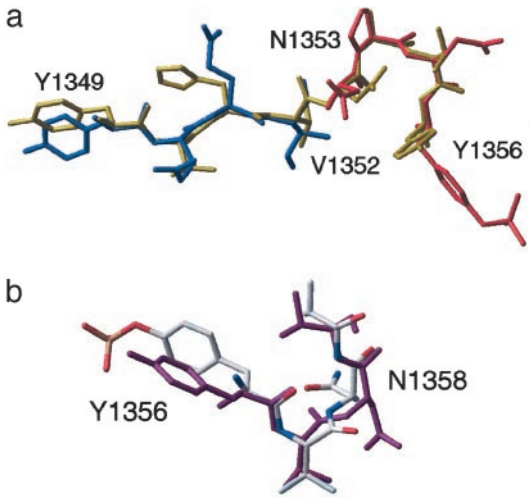

Fig. 3. (*a*) Residues 1349–1356 of the C-terminal supersite of c-Met (yellow). Superimposed are tetrapeptides from phosphopeptide complexes of the SH2 domain of Lck (PDB ID code 1LCJ; ref. 41) in blue, and of the PTB domain of Shc (PDB ID code 1SHC; ref. 42) in red. (*b*) Comparison of the β-turn conformation of residues 1356–1359 in c-Met (magenta) to residues pYVNV of a phosphopeptide complex of Grb2 (gray carbon atoms; PDB ID code 1TZE; ref. 39).

In our structures, neither of the tyrosines are phosphorylated. The protein chain is in an extended conformation for residues 1349–1352, followed by two β-turns, 1353–1356 and 1356–1359. The first tyrosine motif assumes an extended geometry as in phosphopeptides bound to canonical SH2 domains. Fig. 3*a* shows the extended phosphopeptide as bound to the Lck SH2 domain (41), which is superimposed on residues 1349–1352 of c-Met. The orientation of the segment 1349–1352 is such that binding of the Lck-SH2 domain would lead to an overlap with parts of the c-Met C lobe, suggesting that during c-Met activation, the SH2-interacting residues would need to reorient toward the surface of the kinase.

The residues ^{1353}NATY fold as a type I β-turn. The sequence of this motif is similar to the consensus sequence for Shc-PTB domain-binding peptides (NPXY). The NMR structure of the PTB domain of a Shc:peptide complex showed the NPXpY motif at the C terminus of a β-strand forming a type I β-turn structure (42). Superposition of this β-turn onto the C^{α} positions of c-Met 1353–1356 shows a high degree of conformational similarity between both β-turns with a C^{α} rms deviation of 0.18 Å (Fig. 3*a*). Also, in this case, docking of the PTB domain would lead to steric clashes with the kinase C lobe.

Tyr-1356 and the three residues that follow it form a type II β-turn. Phosphopeptides bind to Grb2 in a type I β-turn conformation, which is related to type II β-turns by a 180° flip of the central peptide unit. Fig. 3*b* shows this segment for c-Met in comparison to the same sequence of a phosphopeptide bound to Grb2 SH2 (39). Conformational differences concern the φ-dihedral angle of Tyr-1356 and its side chain rotamer, as well as a peptide flip for the bond between Val-1357 and Asn-1358. A change in rotamer conformation would move the Asn-1358 side chain into its position in the Grb2-complex. In this case, the SH2 domain of Grb2 can be docked to c-Met by superimposing its bound peptide with c-Met residues 1356–1359 without significant steric clashes with the c-Met C-lobe. The presence of these three motifs in conformations close to those recognized by their binding partners implies that the conformation of the C-terminal supersite in our crystal structure shares elements with its structure in active, full-length c-Met.

Mutations in Cancer. In several human cancers, point mutations in the c-Met kinase domain have been detected, and have been shown to lead to kinase activation *in vitro* (see introduction; for a review, see ref. 14). Fig. 1*a* maps the following point mutations onto the c-Met kinase domain: V1092I, H1094L/Y/R, H1106D, M1131T, V1188L, L1195V, V1220I, D1228H/N, Y1230H/C, Y1235D, K1244R, and M1250T/I. Although it is difficult to predict with any certainty the effects of these mutations, some of them would appear to affect the conformation of the A loop. In an active kinase, the A loop takes a particular conformation in which substrate and nucleotide can bind. In wild-type c-Met, phosphorylation of tyrosines 1234 and 1235 shifts the A-loop equilibrium toward the active conformation. Mutations may affect either the stability of the active conformation or destabilize the inactive conformation. An example of the former is the Y1235D mutation, for which we have solved the structure. This mutation is expected to mimic the negative charge of the phosphotyrosine. Our c-Met sample is unphosphorylated and enzymatically active and must be able to adopt an active conformation of the A loop. Nevertheless, in our structure, a unique, inactive A-loop conformation is present, with the segment including Asp-1235 blocking peptide substrate binding. In addition, the segment 1223–1226 bulges up to the N lobe, constraining helix αC in an inactive orientation, and residues 1228–1230 are in a position that would interfere with nucleotide binding. The mutations involving residues Met-1131, Leu-1295, Asp-1228, and Tyr-1230 might destabilize this inactive conformation. Met-1131 and Leu-1195 directly participate in the hydrophobic pocket harboring the Phe-1223 side chain, and Met-1131 is, in addition, in van der Waals contact with Leu-1225. Replacing these residues by threonine and valine will diminish the hydrophobic contacts and make the inactive conformation of the immediate N-terminal portion of the A loop less favorable. Met-1131 and Leu-1195, together with Val-1220, are also involved in a hydrophobic interface between the N lobe, C lobe, and A loop. Their mutations could trigger conformational adaptations of the subdomains that communicate through this interface, aiding in the transition to an active kinase conformation.

Val-1092 is a hydrophobic residue in the adenosine-binding cleft, and is also one of the residues that make van der Waals contacts with K-252a (Fig. 2). An increase in enzymatic activity by the replacement with an isoleucine might be due to an effect on nucleotide binding. Met-1250 is also conserved in insulin receptor and FGFRK, and is in an area of the structure with high sequence and structural similarity among these kinases. c-Met residues 1245–1253 superimpose with a C^{α} rms deviation of 0.3 Å with the respective residues in the ternary complex of insulin receptor, including substrate peptide (37). In insulin receptor, the corresponding methionine is involved in substrate binding. A mutation of Met-1250 might thus have an effect on peptide binding. This possibility was also previously suggested in a modeling study discussing potential effects of cancer mutations on the c-Met structure, based on the structures of IRK and IRK3P (43).

The structure of c-Met provides additional illustration for the plasticity of protein kinase structures and adds another example of a tyrosine kinase in complex with an indolocarbazole inhibitor. It reveals a conformation of the A loop that contributes with its N-terminal residues to the K-252a-binding site, showing conformational adaptability to indolocarbazole binding. Targeting this subsite might, therefore, aid in the design of specific inhibitors for c-Met. Our study provides structural information for the c-Met kinase domain, including a mutation found in human cancer (Y1235D), and allows mapping of other cancer-related mutations. It elucidates the position and conformation of the C-terminal c-Met supersite in its nonphosphorylated form, allowing to derive a plausible binding orientation for interaction of the Grb2 SH2 domain with the second tyrosine motif. Two additional motifs of the supersite are in a conformation seen in complexes with SH2- and PTB-domain-containing binding partners. A confirmation of the relevance of the conformation of the supersite reported here has to await structure determinations of c-Met complexes with intracellular transducers.

We thank Alexander Cameron and Jay Bertrand for discussion and critical reading of the manuscript; A. Cameron and Elena Casale for help with data collection; and Henryk Kalisz, Albert Stewart, Antonella Isacchi, James Christensen, Mario Varasi, Cristiana Marcozzi, Jan Malyszko, Michael Forstner, and Rosario Baldi for discussions and technical support.

1. Trusolino, L. & Comoglio, P. M. (2002) *Nat. Rev. Cancer* **2,** 289–300.
2. Cooper, C. S., Park, M., Blair, D. G., Tainsky, M. A., Huebner, K., Croce, C. M. & Vande Woude, G. F. (1984) *Nature* **311,** 29–33.
3. Dean, M. M., Park, M. M., Le Beau, T. S., Robins, T. S., Diaz, M. O., Rowley, J. D., Blair, D. G. & Vande Woude, G. F. (1985) *Nature* **318,** 385–388.
4. Bottaro, D. P., Rubin, J. S., Faletto, D. L., Chan, A. M. L., Kmiecick, T. E., Vande Woude, G. F. & Aaronson, S. A. (1991) *Science* **251,** 802–804.
5. Birchmeier, C. & Gherardi, E. (1998) *Trends Cell Biol.* **8,** 404–410.
6. Maulik, G., Shrikhande, A., Kijima, T., Ma, P. C., Morrison, P. T. & Salgia, R. (2002) *Cytokine Growth Factor Rev.* **13,** 41–59.
7. Naldini, L., Vigna, E., Ferracini, R., Longati, P., Gandino, L., Prat, M. & Comoglio, P. M. (1991) *Mol. Cell. Biol.* **11,** 1793–1803.
8. Ferracini, R., Longati, P., Naldini, L., Vigna, L. & Comoglio, P. M. (1991) *J. Biol. Chem.* **266,** 19558–19564.
9. Ponzetto, C., Bardelli, A., Zhen, Z., Maina, F., Dalla Zonca, P., Giordano, S., Graziani, A., Panayotou, G. & Comoglio, P. M. (1994) *Cell* **77,** 261–271.
10. Comoglio, P. M. (2001) *Nat. Cell Biol.* **3,** 161–162.
11. Maina, F., Casagranda, F., Audero, E., Simeone, A., Comoglio, P. M., Klein, R. & Ponzetto, C. (1996) *Cell* **87,** 531–542.
12. Furge, K. A., Zhang, Y. & Vande Woude, G. F. (2000) *Oncogene* **19,** 5582–5589.
13. Saucier, C., Papavasiliou, V., Palazzo, A., Naujokas, M. A., Kremer, R. & Park, M. (2002) *Oncogene* **21,** 1800–1811.
14. Danilkovitch-Miagkov, A. & Zbar, B. (2002) *J. Clin. Invest.* **109,** 863–867.
15. Wood, J. L., Stoltz, B. M., Dietrich, H.-J., Pflum, D. A. & Petsch, D. T. (1997) *J. Am. Chem. Soc.* **119,** 9641–9651.
16. Prade, L., Engh, R. A., Girod, A., Kinzel, V., Huber, R. & Bossemeyer, D. (1997) *Structure (London)* **5,** 1627–1636.
17. Lawrie, A. M., Noble, M. E. M., Tunnah, P., Brown, N. R., Johnson, L. N. & Endicott, J. A. (1997) *Nat. Struct. Biol.* **4,** 796–801.
18. Lamers, M. B. A. C., Antson, A. A., Hubbard, R. E., Scott, R. K. & Williams, D. H. (1999) *J. Mol. Biol.* **285,** 713–725.
19. Zhu, X., Kim, J. L., Newcomb, J. R., Rose, P. E., Stover, D. R., Toledo, L. M., Zhao, H. & Morgenstern, K. A. (1999) *Structure (London)* **5,** 651–661.
20. Huse, M. & Kuriyan, J. (2002) *Cell,* **109,** 275–282.
21. Scarpin, G. (2002) *Drug Discov. Today*, **7,** 601–611.
22. Kase, H., Iwahashi, K., Nakanishi, S., Matsuda, Y., Yamada, K., Takahashi, M., Murakata, C., Sato, A. & Kaneko, M. (1987) *Biochem. Biophys. Res. Commun.* **142,** 436–440.
23. Ruggeri, B. A., Miknyoczki, S. J., Singh, J. & Hudkins, R. L. (1999) *Curr. Med. Chem.* **6,** 845–857.
24. Morotti, A., Mila, S., Accornero, P., Tagliabue, E. & Ponzetto, C. (2002) *Oncogene* **21,** 4885–4893.
25. Di Renzo, M. F., Olivero, M., Martone, T., Maffe, A., Maggiora, P., De Stefani, A., Valente, G., Giordano, S., Cortesina, G. & Comoglio, P. M. (2000) *Oncogene* **19,** 1547–1555.
26. Otwinowski, Z. & Minor, W. (1997) *Methods Enzymol.* **276,** 307–326.
27. Kissinger, C. R., Gehlhaar, D. K. & Fogel, D. B. (1999) *Acta Crystallogr. D* **55,** 484–491.
28. Jones, T. A., Zou, J. Y., Cowan, S. W. & Kjeldgaard, M. (1991) *Acta Crystallogr. A* **47,** 110–119.
29. Brünger, A. T., Adams, P. D., Clore, G. M., DeLano, W. L., Gros, P., Grosse-Kunstleve, R. W., Jiang, J. S., Kuszewski, J., Nilges, M., Pannu, N. S., *et al.* (1998) *Acta Crystallogr. D* **54,** 905–921.
30. Collaborative Computational Project 4 (1994) *Acta Crystallogr. D* **50,** 760–776.
31. Perrakis, A., Morris, R. & Lamzin, V. S. (1999) *Nat. Struct. Biol* **5,** 458–463.
32. Laskovsky, R. A., MacArthur, M. W., Moss, D. & Thornton, J. M. (1993) *J. Appl. Crystallogr.* **26,** 283–291.
33. Mohammadi, M., McMahon, G., Sun, L., Tang, C., Hirth, P., Yeh, B. K., Hubbard, S. R. & Schlessinger, J. (1997) *Science* **276,** 955–960.
34. Mohammadi, M., Schlessinger, J. & Hubbard, S. R. (1996) *Cell* **86,** 577–587.
35. Hubbard, S. R., Wei, L., Ellis, L. & Hendrickson, W. A. (1994) *Nature* **372,** 746–754.
36. Hubbard, S. R. (1997) *EMBO J.* **16,** 5573–5581.
37. Knighton, D. R., Zheng, J., Ten Eyck, L. F., Ashford, V. A., Xuong, N., Taylor, S. S. & Sowadski, J. M. (1991) *Science* **253,** 407–414.
38. Kuriyan, J. & Cowburn, D. (1997) *Annu. Rev. Biophys. Biomol. Struct.* **26,** 259–288.
39. Rahuel, J., Gay, B., Erdmann, D., Strauss, A., García-Echevírra, C., Furet, P., Caravatti, G., Fretz, H., Schoepfer, J. & Grütter, M. G. (1996) *Nat. Struct. Biol.* **3,** 586–589.
40. Schiering, N., Casale, E., Caccia, P., Giordano, P. & Battistini, C. (2000) *Biochemistry* **39,** 13376–13382.
41. Eck, M. J., Shoelson, S. E. & Harrison, S. C. (1993) *Nature* **362,** 87–91.
42. Zhou, M. M., Ravichandran, K. S., Olejniczak E. F., Petros, A. M., Meadows, R. P., Harlan, J. E., Sattler, M., Wade, W. S., Burakoff, S. J. & Fesik, S. W. (1995) *Nature* **378,** 584–592.
43. Miller, M., Ginalski, K., Lesyng, B., Nakaigawa, N., Schmidt, L. & Zbar B. (2001) *Proteins Struct. Funct. Genet.* **44,** 32–43.
44. Abagyan, R. A., Totrov, M. M., Kuznetsov, D. N. (1994) *J. Comput. Chem.* **15,** 488–506.
45. Mroczkowski, B., Hickey, M., McTigue, M. A., Murray, B. W., Parge, H., Sarup, J. & Zhu, J. (2002) Eur. Patent Appl. EP 1 243 5a6 A2.